PHYSICAL REVIEW B **85**, 081301(R) (2012)

Resonance-hybrid states in a triple quantum dot

S. Amaha,[1,2,*] T. Hatano,[1,3] H. Tamura,[4] S. Teraoka,[1,5] T. Kubo,[1,4] Y. Tokura,[1,4] D. G. Austing,[6] and S. Tarucha[1,5]

[1]*Quantum Spin Information Project, Japan Science and Technology Agency, International Cooperative Research Project (ICORP), 3-1, Morinosato, Wakamiya, Atsugi, Kanagawa 243-0198, Japan*

[2]*Low Temperature Physics Laboratory, RIKEN, 2-1 Hirosawa, Wako, Saitama 351-0198, Japan*

[3]*Nuclear Spin Electronics Project, Japan Science and Technology Agency, Exploratory Research for Advanced Technology (ERATO), Aoba, Aramaki, Sendai, Miyagi 980-8578, Japan*

[4]*NTT Basic Research Laboratories, NTT Corporation, 3-1, Morinosato, Wakamiya, Atsugi, Kanagawa 243-0198, Japan*

[5]*Department of Applied Physics, School of Engineering, University of Tokyo, 7-3-1, Hongo, Bunkyo-ku, Tokyo 113-8656, Japan*

[6]*National Research Council of Canada, Institute for Micro-structural Sciences M50, Montreal Road, Ottawa, Ontario, Canada K1A 0R6*

(Received 6 January 2012; published 2 February 2012)

Delocalization by resonance between contributing structures explains the enhanced stability of *resonance-hybrid* molecules. Here we report the realization of resonance-hybrid states in a few-electron triple quantum dot (TQD) obseved by excitation spectroscopy. The stabilization of the resonance-hybrid state and the bond between contributing states are achieved through access to the intermediate states with double occupancy of the dots. This explains why the energy of the hybridized singlet state is significantly lower than that of the triplet state. The properties of the three-electron doublet states can also be understood with the resonance-hybrid picture and geometrical phase. As well as for fundamental TQD physics, our results are useful for the investigation of materials such as quantum dot arrays, quantum information processors, and chemical reaction and quantum simulators.

DOI: 10.1103/PhysRevB.85.081301 PACS number(s): 73.63.Kv, 73.23.Hk

Enhanced stability by resonance between two or more contributing structures in molecules and solids can be understood within the framework of a *resonance hybrid*[1] and a *resonating valence bond* (RVB).[2] The most familiar examples are benzene, ozone, and nitrogen dioxide. The concept is important to understand bond strength, molecular stuctures, and chemical reactions. On the other hand, quantum dots (QDs) are widely known to show atomiclike properties. By using QDs as building blocks, multiple QD systems can allow us to explore quantum effects seen in real molecules and solids. Many theoretical works have investigated multiple QDs for materials such as QD arrays,[3,4] and for quantum information processors[5–13] and chemical reaction and quantum simulators.[14,15] Following progress in fabrication technologies, there are now significant efforts to exploit triple QDs (TQDs),[16–27] quadruple QDs,[28] and artificial QD lattices[29] for unique physics and applications. An attractive capability of multiple QD systems is the *continuous* tunability of parameters, e.g., the tunnel coupling strength and electrochemical potentials, with gate voltages. The number of electrons and the arrangement of artificial atom QDs are also not limited by physical and chemical constraints. Additionally, toward the implementation of multiple qubits, the manipulation of three-electron spins in TQDs has also become an active topic[25–27] and the experimental study of spin states in TQDs has become important. Moreover, the RVB state is regarded as a candidate for topological qubits with fault-tolerant Abelian states,[30] thus the realization of RVB states in multiple QD systems is potentially an important step for the implementation of topological qubits.

Here we report on resonance-hybrid states in a few-electron TQD and explore the origin of the resonance-hybrid bond stability focusing on spin. The observed evolution of the two- and three-electron ground- and excited-state electrochemical potentials are well accounted for with a three-site Hubbard model. The stability of two-electron singlet and three-electron doublet states is explained with the resonance-hybird picture.

Our TQD is embedded inside three collinearly connected submicrometer rectangular mesas [Figs. 1(a) and 1(b)]. The sizes of the mesas are adjusted to attain the few-electron regime in each QD (dots 1, 2, and 3). The four separate gate electrodes (G_1, G_2, $G_{2'}$, G_3) principally control the electrochemical potentials of the three QDs. We measure at ∼100 mK the dc current I flowing from the source (substrate) contact into the three QDs in parallel and out to the drain electrode under a constant source-drain bias V_{sd} applying voltages (V_{g1}, V_{g2}, $V_{g2'}$, V_{g3}) to (G_1, G_2, $G_{2'}$, G_3). $V_{g2'} = V_{g2}$ and the magnetic field is zero. A unique feature of our TQD is that the QDs are arranged in parallel rather than in series between the source and drain. This allows us to measure current and observe states even if all QDs are not simultaneously on resonance [Fig. 1(c)].

Figure 1(d) shows dI/dV_{g1} in the V_{g1}-V_{g2} plane for $V_{g3} = -0.38$ V. V_{sd} is sufficiently small to observe the evolution of just the ground-state electrochemical potentials. To the lower left, we identify the region where the total number of electrons in the TQD, N, is zero. We can straightforwardly determine charge configurations for the Coulomb blockaded regions (N_1, N_2, N_3) from the slope ($\Delta V_{g1}/\Delta V_{g2}$) of each Coulomb oscillation line away from the anticrossing regions, where the number of electrons in dots 1, 2, and 3 are N_1, N_2, and N_3, respectively. The separation between, and "rounding" of, the two Coulomb oscillation lines at anticrossing regions (the most relevant are X, Y, and Z) demonstrate finite interdot Coulomb interaction and tunnel coupling. The lowest single-particle energy levels in dots 1 and 2 (dots 2 and 3) are in close alignment at X (Y), whereas the levels in dots 1 and 3 are aligned near Z.

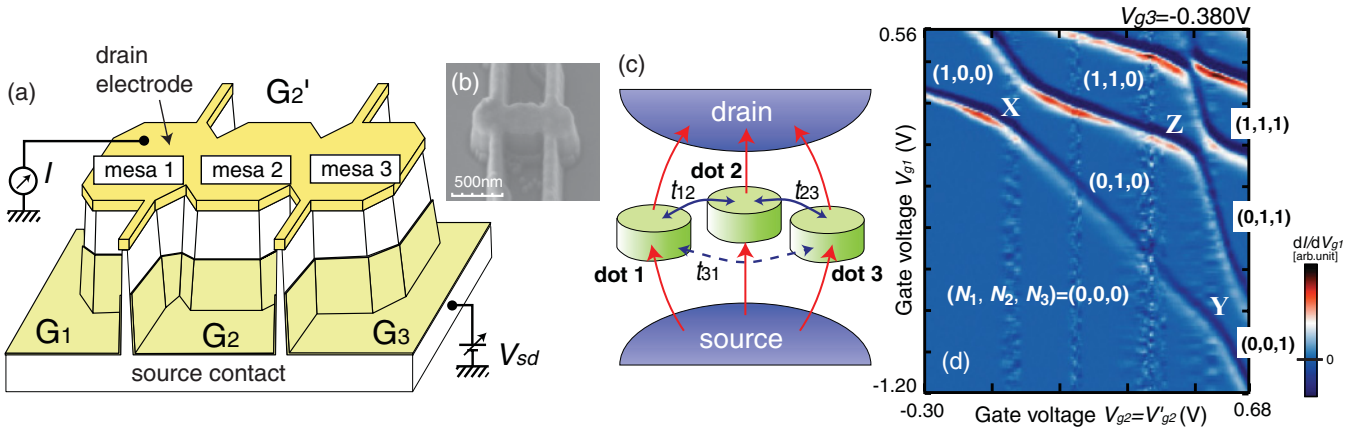

FIG. 1. (Color online) (a) Schematic of device fabricated from an $Al_{0.3}Ga_{0.7}As/GaAs$ double-barrier resonant tunneling structure. Four thin line mesas connected to the three rectangular mesas define four separate gate electrodes (G_1, G_2, $G_{2'}$, G_3) ($G_{2'}$ hidden from view). (b) Scanning electron micrograph of device similar to the one measured. (c) Cartoon of current flow through TQD. (d) Stability diagram showing dI/dV_{g1} for $N = 0$–4 measured with $V_{g3} = -0.38$ V and $V_{sd} = 300$ μV. The choice to plot dI/dV_{g1} minimizes the influence of charge traps in the thin mesa lines that lead to several extraneous almost vertical features that do not influence the physics of interest.

On increasing V_{sd}, the Coulomb oscillation lines broaden into current stripes [Fig. 2(a)] and excited states within the energy window eV_{sd} become accessible, potentially leading to current enhancement.[31,32] We focus most attention on Z [Fig. 2(b)], where the TQD physics of interest occurs. Beforehand, we apply a Hubbard model (using an exact diagonalization method[20]) to calculate the electrochemical potentials $\mu_g(N=1)$, $\mu_g(2)$, $\mu_e(2)$, $\mu_g(3)$, and $\mu_e(3)$ [g = ground state, e = first excited state, and $\mu(N)$ is the energy of the N electron state minus the energy of the $N-1$ electron ground state[20,31,32] as a function of energy detuning between dots 1 and 3, ε [Fig. 2(c)]. Parameters estimated from experiment reproducing key features are as follows: intradot Coulomb energies U_i of dot i ($i = 1,2,3$), $U_1 = U_2 = U_3 = U = 3.0$ meV; interdot Coulomb energies V_{ij} between dots i and j ($i,j = 1,2,3$, $i \neq j$), $V_{12} = V_{23} = V = 1.0$ meV, and $V_{31} = 0.5$ meV; interdot tunnel coupling energies t_{ij} between dots i and j ($i,j = 1,2,3$, $i \neq j$), $t_{12} = t_{23} = -0.2$ meV, and $t_{31} = -0.05$ meV; lowest single-particle energy level E_i in each dot i ($i = 1,2,3$), $E_1 = 0.5\varepsilon$, $E_2 = \delta$ ($=-1.5$ meV), and $E_3 = -0.5\varepsilon$ (only one single-particle level in each QD is assumed). δ represents an ε-independent energy offset for dot 2. In Fig. 2(c) we plot the ground state and the first excited state with spin different from the ground state (except the $N = 3$ first excited doublet) state to reproduce our experiment. Fast relaxation from excited states to the ground state prevents their detection by excitation spectroscopy.[33] The details on the relaxation are discussed later.

We now discuss the $N = 2$ states [Fig. 2(b)]. Close to X (Y), the ground and first excited states, respectively, are the singlet $|S_{12}\rangle$and triplet $|T_{12}\rangle$ ($|S_{23}\rangle$ and $|T_{23}\rangle$) with one electron each on dots 1 and 2 (dots 2 and 3), as expected from double QD spin physics.[32,34] When ε approaches zero (close to Z), $|S_{12}\rangle$ and $|S_{23}\rangle$ ($|T_{12}\rangle$ and$|T_{23}\rangle$) become resonant, the energy separation between the $N = 2$ singlet and triplet levels [$\mu_g(2)$ and $\mu_e(2)$] increases, and the (negative) curvature of $\mu_g(2)$ is always much weaker than that of $\mu_e(2)$. The coupling strength between (1,1,0) and (0,1,1) determining the curvature can be evaluated by considering transitions from (1,1,0) to (0,1,1) via the tunneling Hamiltonian. The perturbative processes that hybridize (1,1,0) and (0,1,1) are identified as a first-order (direct) tunneling process, t_{31}^*, (1,1,0) $\rightarrow$ (0,1,1), plus second-order tunneling processes involving intermediate states. In the second-order tunneling processes, the transitions from (1,1,0) to (0,1,1) are achieved by two consecutive electron transfer processes. They are limited to (1,1,0) $\rightarrow$ (1,0,1) $\rightarrow$ (0,1,1) and (1,1,0) $\rightarrow$ (0,2,0) $\rightarrow$ (0,1,1).[35] Note that (1,0,1) and (0,2,0) are not *real* but *virtual* states in the transfer process. For the $|t_{12}| \sim |t_{23}| > |t_{31}|$ regime, the second-order processes become important when the energy difference ($\Delta E > 0$) between the intermediate state (1,0,1) or (0,2,0) and initial state (1,1,0) [or (0,1,1)] is small. Both the singlet and triplet resonances can access the intermediate state (1,0,1), but its contribution is generally small since (1,0,1) is higher in energy than (1,1,0) and (0,1,1). On the other hand, only the singlet resonance can access the double occupied intermediate state (0,2,0) [Fig. 2(d)], for which ΔE is small due to negative δ. However, for the triplet resonance, the access to (0,2,0) is forbidden by Pauli exclusion without the occupation of a higher-energy orbital in dot 2. Accordingly, the singlet resonance is more stable than the triplet resonance, and the curvature of the former is weaker than that of the latter, reflecting the stronger hybridization between (1,1,0) and (0,1,1) in the singlet case.

Concerning the $N = 3$ states at Z [Fig. 2(b)], we identify two positive curvature levels [$\mu_g(3)$ and $\mu_e(3)$] in the third current stripe. The total spin of both states is $S = 1/2$. In the Heisenberg model for a collinear TQD, the spin states can be also classified by the total spin of two electrons in dots 1 and 3, S' (=0 and 1).[25] The doublet state with $S' = 1$ (D_1) is the ground state and that with $S' = 0$ (D_0) is the first excited state. A quadruplet (Q, $S = 3/2$) state with a charge configuration (1,1,1) is not observed, nor is it expected due to the spin blockade since the $N = 2$ ground state is a singlet.

To demonstrate the importance of contributing states for bond stability in the singlet resonance-hybrid state, we present current stripes for different V_{g3} focusing on $N = 2$ and 3 states close to Z in Figs. 3(a)–3(c).[35] Figures 3(d)–3(f)

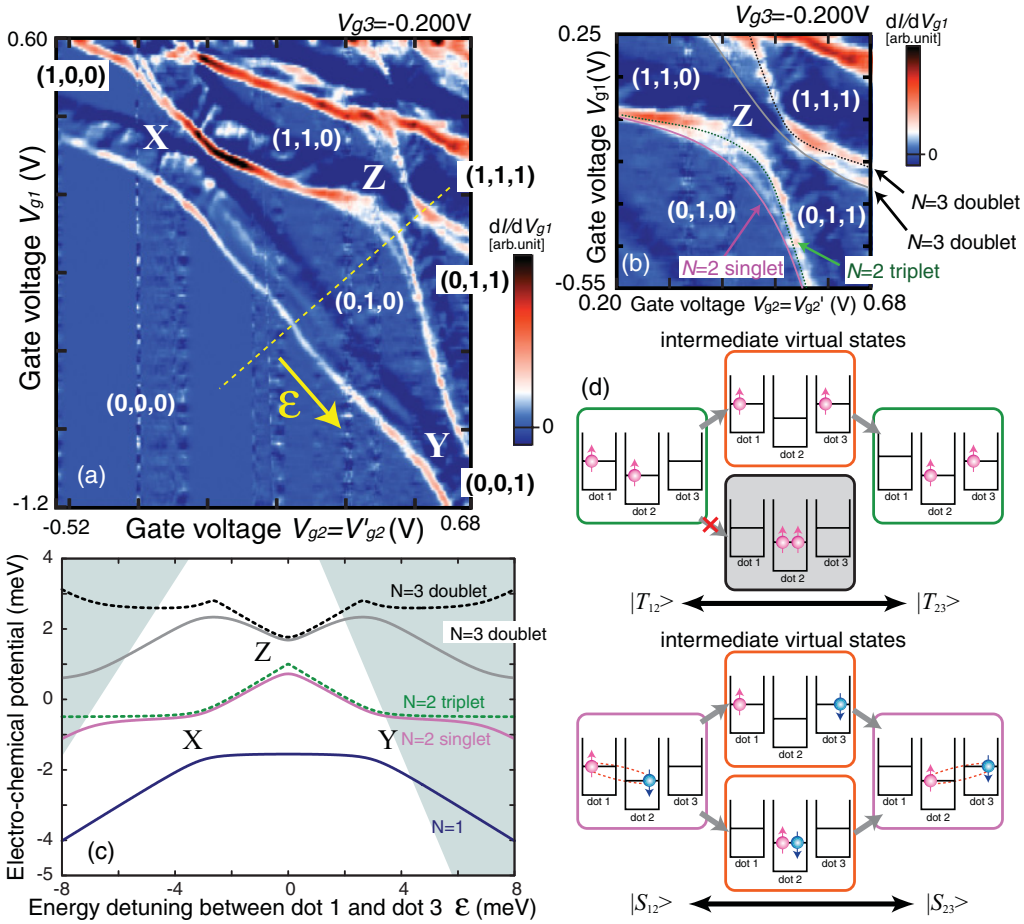

FIG. 2. (Color online) (a) dI/dV_{g1} for $N = 0$–4 measured with $V_{g3} = -0.20$ V and $V_{sd} \sim 1$ mV. (b) Expanded plot in vicinity of Z. (c) Modeled evolution of relevant electrochemical potentials as a function of ε [see (a) for sense of ε]. (d) States participating in triplet (singlet) resonance between $|T_{12}\rangle$ and $|T_{23}\rangle$ ($|S_{12}\rangle$ and $|S_{23}\rangle$).

show the calculated electrochemical potential versus energy detuning maps reproducing the data. As V_{g3} is stepped from $V_{g3} = -0.20$ V [Fig. 2(b)] to +0.50 V [Figs. 3(a)–3(c)], the first current stripe (marked with an asterisk) shifts toward the bottom left in Figs. 3(a)–3(c), therefore we conclude that the (0,1,0) state becomes more stabilized (δ becomes more negative) as V_{g3} becomes positive.[35] At the same time, inside the second current stripe, the separation between the singlet and triplet levels $\mu_g(2)$ and $\mu_e(2)$, increases and the (negative) curvature of $\mu_g(2)$ weakens. Concurrently, inside the third current stripe, the sign of the curvature of level $\mu_g(3)$ changes from positive to negative, while the separation between the two doublet state levels at $\varepsilon = 0$ meV remains small. We stress that the principle effect of changing V_{g3} is to lower the offset energy δ for dot 2 and strengthen the contribution of the intermediate states without strong modification of t_{31} and V_{31}.[35]

To understand our observations, Figs. 4(a)–4(c) show the calculated charge state contributions for the $N = 2$ and 3 ground states with the same values of δ used in Figs. 3(d)–3(f). The $N = 2$ ground state has a dominant configuration (1,1,0) [(0,1,1)] at $\varepsilon < 0$ ($\varepsilon > 0$), and its energy varies as ε ($-\varepsilon$). As δ is made more negative (by making V_{g3} more negative), the negative curvature of level $\mu_g(2)$ is reduced and finally $\mu_g(2)$ becomes almost "flat" near $\varepsilon = 0$ meV [Fig. 3(c)]. The change in curvature of $\mu_g(2)$ with V_{g3} can be understood by the increase in weight of (0,2,0) in $N = 2$ [Figs. 4(a)–4(c)]. A crossover from a dominant charge state of (1,1,0) plus (0,1,1) to (0,2,0) is revealed in Fig. 4(d) on plotting the δ dependence of charge contribution for the $N = 2$ ground state. Neglecting tunneling, the boundary condition for δ where the weight of (0,2,0) dominates that of (1,1,0) and (0,1,1) is $\delta_P = V - U = -2.0$ meV. In Figs. 3(a)–3(c), the separation between $\mu_g(2)$ and $\mu_e(2)$ is observed to increase as δ is reduced by modification of V_{g3}. This increase cannot be due to direct tunneling t_{31} because direct tunneling equally contributes to singlet and triplet states. Instead, the increase is because the resonance-hybrid bond between (1,1,0) and (0,1,1) singlet states is promoted compared to the bond between (1,1,0) and (0,1,1) triplet states by the lowering of the energy of the intermediate state (0,2,0). The access of the intermediate state (0,2,0) is essential for the stabilization of the resonance-hybrid state in the TQD, but access is allowed only for the singlet state. The observed difference in curvature between the singlet and triplet levels at Z is a consequence of the stabilization by the resonance hybrid state, i.e., the stronger stabilization of the singlet observed at Z demonstrates the realization of the resonance hybrid state for the singlet.

For the $N = 3$ doublet states, making δ more negative stabilizes charge configurations (1,2,0) and (0,2,1) relative to (1,1,1). Figure 4(d) shows the δ dependence of the charge

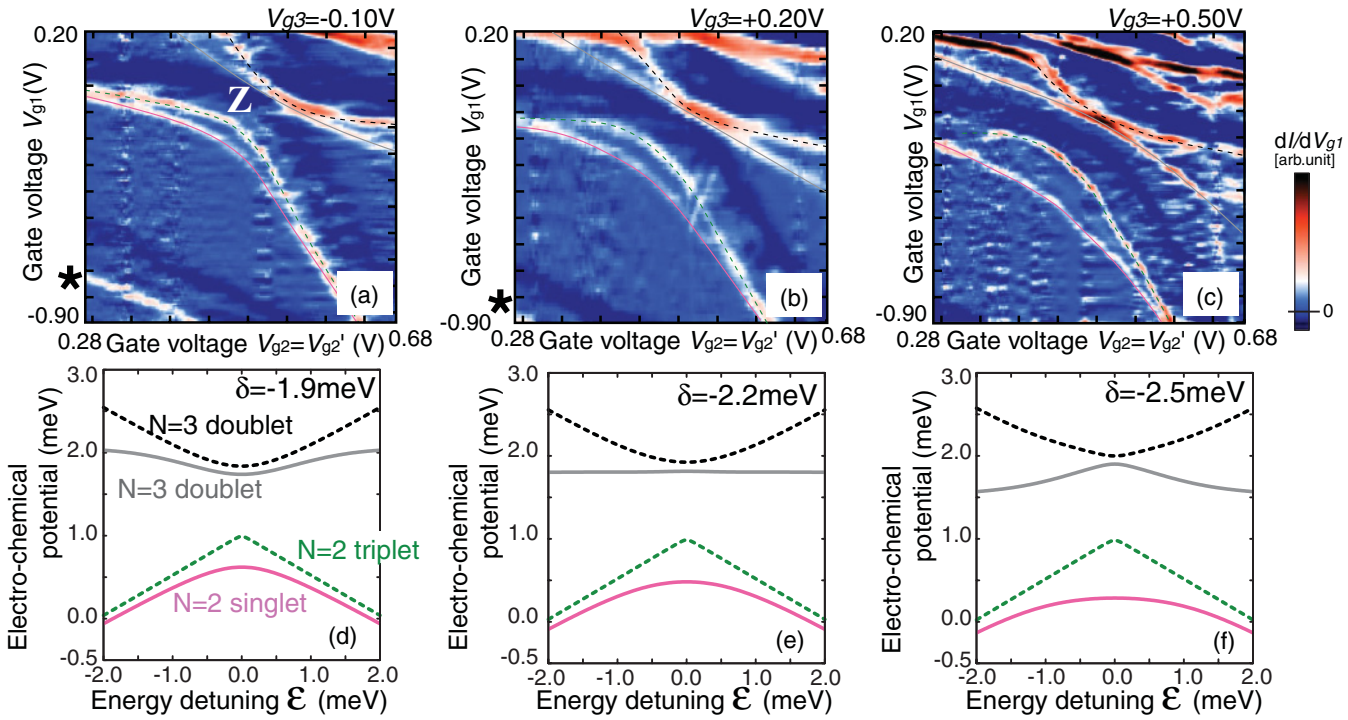

FIG. 3. (Color online) Modulation of stability diagram near Z by tuning voltage V_{g3}. dI/dV_{g1} with (a) $V_{g3} = -0.1$ V, (b) $V_{g3} = +0.2$ V, and (c) $V_{g3} = +0.5$ V. V_{sd} is ~1 mV. Note that part of the first current stripe (marked with an asterisk) shifts out of view in (c). Calculated electrochemical potential vs energy detuning ε maps for $N = 2$ and 3 states with (d) $\delta = -1.9$ meV, (e) $\delta = -2.2$ meV, and (f) $\delta = -2.5$ meV. All other parameters are the same as those for Fig. 2(c).

contributions for the $N = 3$ ground state. The (1,1,1) charge contribution is less dominant for $\delta < \delta_Q$ (neglecting tunneling, $\delta_Q = V_{31} - U = -2.5$ meV). δ_P and δ_Q are different because $V(=V_{12} = V_{23})$ and V_{31} are not the same, and this influences the behavior of $\mu_g(3)$ near Z. When $\delta_P < \delta$, (1,1,1) is the dominate charge configuration [Fig. 4(a)]. $\mu_g(3)$ near $\varepsilon = 0$ meV is expected to have a positive curvature as found in Figs. 3(a) and 3(d), because the energy of (1,1,1) is independent of ε, and the $N = 2$ ground state with charge configurations (1,1,0) and (0,1,1), respectively, has energy varying as ε and $-\varepsilon$. When $\delta_Q < \delta < \delta_P$, the charge configuration (0,2,0) gains weight [Fig. 4(b)], and since (1,1,1) energy is independent of ε, $\mu_g(3)$ "flattens," as is evident in Figs. 3(b) and 3(e). When $\delta < \delta_Q$, the charge configurations (1,2,0) and (0,2,1) gain weight [Fig. 4(c)], and since they have energies varying as ε and $-\varepsilon$, respectively, $\mu_g(3)$ has negative curvature, as seen in Figs. 3(c) and 3(f).

We also comment on the calculated relaxation times T_1 relevant to our experiment. If T_1 from the excited state to the ground state is longer than the escape time from the TQD, an additional current step associated with the excited state can be observed.[33] Generally T_1 between different spin states is sufficiently long to be observed in the excitation spectra.[33] Consequently, it should be necessary to plot the electrochemical potential of only the first excited state with different spin from the ground state in Fig. 2(c). However, the current step associated with the first excited $N = 3$ doublet state is clearly observed in Figs. 2(a)–2(c), even though the excited state has the same total spin S as the $N = 3$ ground state. To understand why, we calculated T_1 with the electron-phonon interaction as shown in Figs. 4(a)–4(c).[35] In each case, T_1 for $N = 3$ is comparable to $1/\Gamma \sim 10^{-10}$ s, where Γ is the tunneling rate to the source and drain electrodes [typically a few μeV in our QD devices],[32] and it is longer ($\sim\times 10^2$) than T_1 for $N = 1$ at X (between symmetric and antisymmetric states), so we expect to observe the step from the first excited doublet state in the current stripe. There are two main reasons why the relaxation between the two doublet states for $N = 3$ is comparatively slow: (i) D_1 and D_0 have different S' so they cannot be hybridized by electron-phonon coupling; and (ii) the contribution of hybridized (1,2,0) and (0,2,1) states to the wave function induces electron-phonon coupling, but its weight is less than 1/4. Moreover, the relative weight of the electron in dot 1 (dot 3) is 1/3 compared to that for $N = 1$, which causes additional suppression in electron-phonon coupling $(1/3)^2$.[35]

Finally we observe that the separation between two doublet states remains small in Figs. 3(a)–3(c). Figure 4(e) shows the δ dependence of the electrochemical potential for the ground and first excited doublet states, and the quadruplet state Q. One reason why the separation between the two doublets stays small in contrast to the separation between the ground state and Q is the difference in the accessibility of (1,2,0) and (0,2,1). In the resonance-hybrid picture both D_1 and D_0 are stabilized, but Q is not. Another reason is the geometrical phase associated with the fermionic nature of the electron. Two doublet states D_0 and D_1 are formed when $\delta \gg \delta_Q$ and the symmetric (S) and antisymmetric (AS) states of (1,2,0) and (0,2,1) are formed when $\delta \ll \delta_Q$, and they hybridize when $\delta \sim \delta_Q$. One might expect that D_1 should hybridize with the S state from the permutation process of electrons in dots 1 and 3, but this is not

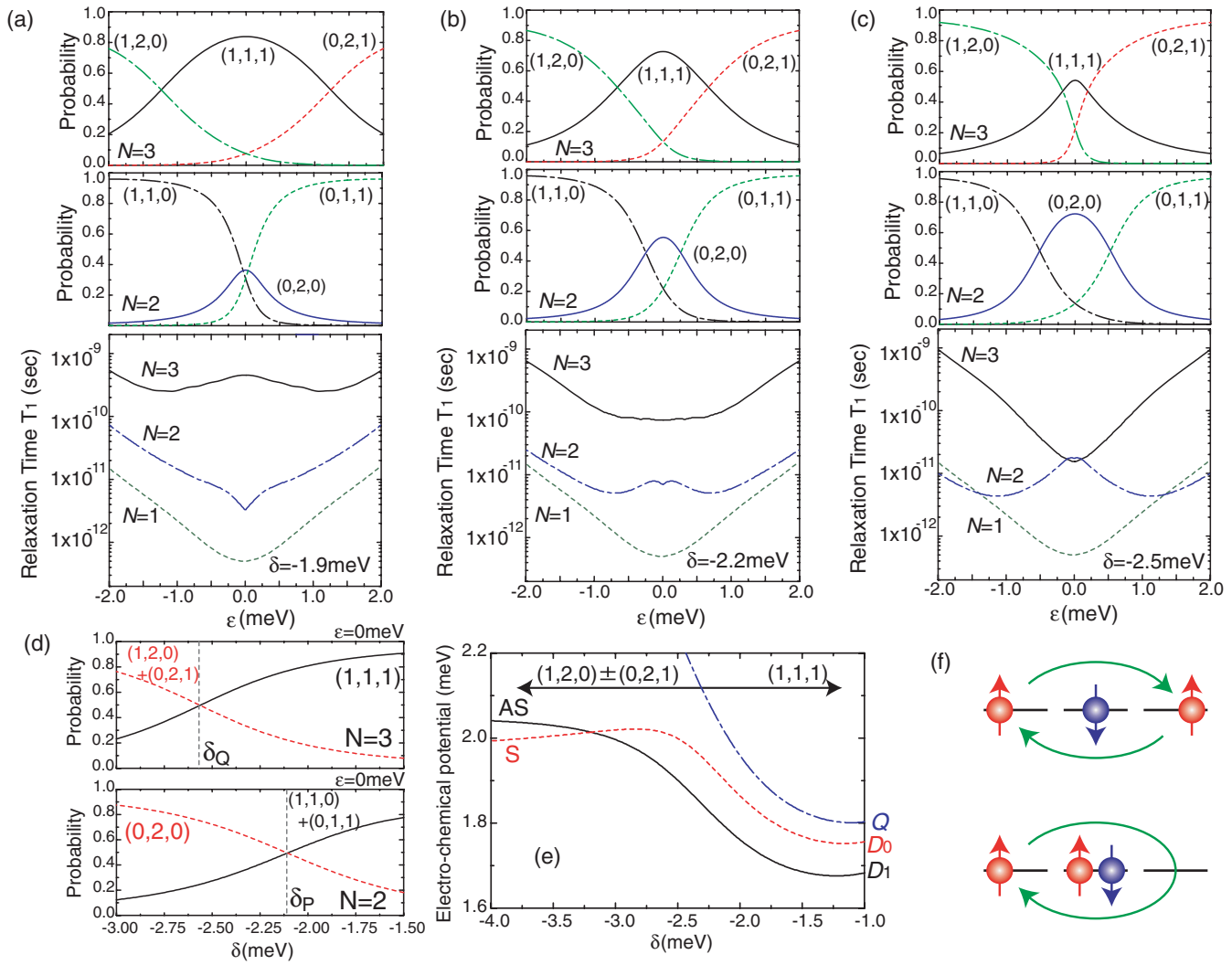

FIG. 4. (Color online) (a)–(c) Calculated weights of ground-state wave function and relaxation time T_1 from the same spin excited state for $N = 2$ and 3 states near Z for $\delta = -1.9$, -2.2, and -2.5 meV. A representative T_1 for $N = 1$ at X for $\delta = -2.0$ meV with an appropriate shift in ε is also plotted for reference. (d) Calculated weights of $N = 2$ ($N = 3$) charge states contributing to singlet (lower doublet) resonance vs δ for $\varepsilon = 0$ meV. (e) Calculated δ dependence of electrochemical potentials for $N = 3$ doublet and quadruplet states. (f) Schematics of the permutation process of electrons in dots 1 and 3 for (1,1,1) and (1,2,0).

so due to additional geometrical phase. For the processes of permutation of electrons in dots 1 and 3 indicated in Fig. 4(f), in the case of (1,1,1), there is an additional phase gain of π from the single electron in dot 2 ("spectator" electron[20]), but for the case of (1,2,0), additional phase is not gained. This phase effect leads to an unusual hybridizing pattern [hybridization of D_1 and the AS state (and of D_0 and the S state)] and level crossing. This keeps the energy separation between the two doublet states small over a wide range of δ [Fig. 4(e)]. From a quantum computation aspect, the level crossing in Fig. 4(e) may facilitate the transition from a superposed state in the S (AS) state, a charge qubit, to that of D_1 (D_0), a spin qubit, by manipulating δ adiabatically.[36]

In conclusion, we explored few-electron states in a collinearly coupled vertical TQD. Enhanced stability of the (1,1,0) ↔ (0,1,1) singlet resonance over the triplet resonance was observed due to the difference in accessibility of the (0,2,0) intermediate state. The evolution of the three-electron ground- and excited-state energies was also understood from the accessibility of (1,2,0) and (0,2,1) intermediate states with the resonance-hybrid picture and geometrical phase in the electron hopping process. Our results provide useful information for spin manipulation in TQDs toward quantum computation, and the realization of resonance-hybrid states is an important step to explore physics in resonance-hybrid molecules and RVB states toward functional materials and topological quantum computation with multiple QDs.

We thank S. V. Nair, T. Maruyama, K. Ono, and K. Kono for useful comments. Part of this work is supported by JSPS Grant-in-Aid for Young Scientists B (No. 23740248) and S (No. 19104007), MEXT Grant-in-Aid for Scientific Research on Innovative Areas (21102003) and Project for Developing Innovation Systems (NanoQuine), Funding Program for World-Leading Innovative R&D on Science and Technology (FIRST), and IARPA project "Multi-Qubit Coherent Operations" through Harvard University.

*Corresponding author: s-amaha@riken.jp

[1] L. Pauling, in *The Nature of the Chemical Bond—An Introduction to Modern Structural Chemistry* (Cornell University Press, Ithaca, NY, 1960), p. 10.
[2] P. W. Anderson, Mater. Res. Bull. **8**, 153 (1973).
[3] C. A. Stafford, R. Kotlyar, and S. Das Sarma, Phys. Rev. B **58**, 7091 (1998).
[4] H. Tamura, K. Shiraishi, T. Kimura, and H. Takayanagi, Phys. Rev. B **65**, 085324 (2002).
[5] D. S. Saraga and D. Loss, Phys. Rev. Lett. **90**, 166803 (2003).
[6] D. P. DiVincenzo, D. Bacon, J. Kempe, G. Burkard, and K. B. Whaley, Nature (London) **408**, 339 (2000).
[7] V. W. Scarola, K. Park, and S. Das Sarma, Phys. Rev. Lett. **93**, 120503 (2004).
[8] A. D. Greentree, J. H. Cole, A. R. Hamilton, and L. C. L. Hollenberg, Phys. Rev. B **70**, 235317 (2004).
[9] B. Michaelis, C. Emary, and C. W. J. Beenakker, Europhys. Lett. **73**, 677 (2006).
[10] K. Le Hur, P. Recher, E. Dupont, and D. Loss, Phys. Rev. Lett. **96**, 106803 (2006); Y.-P. Shim and P Hawrylak, Phys. Rev. B **78**, 165317 (2008).
[11] J. Kim, D. V. Melnikov, J. P. Leburton, D. G. Austing, and S. Tarucha, Phys. Rev. B **74**, 035307 (2006).
[12] M. Busl, R. Sanchez, and G. Platero, Phys. Rev. B **81**, 121306 (2010).
[13] M. Busl and G. Platero, Phys. Rev. B **82**, 205304 (2010).
[14] A. Yu. Smirnov, S. Savel'ev, L. G. Mourokh, and F. Nori, Europhys. Lett. **80**, 67008 (2007).
[15] I. Buluta and F. Nori, Science **326**, 108 (2009).
[16] F. R. Waugh, M. J. Berry, D. J. Mar, R. M. Westervelt, K. L. Campman, and A. C. Gossard, Phys. Rev. Lett. **75**, 705 (1995).
[17] A. Vidan, R. M. Westervelt, M. Stopa, M. Hanson, and A. C. Gossard, Appl. Phys. Lett. **85**, 3602 (2004).
[18] L. Gaudreau, S. A. Studenikin, A. S. Sachrajda, P. Zawadzki, A. Kam, J. Lapointe, M. Korkusinski, and P. Hawrylak, Phys. Rev. Lett. **97**, 036807 (2006).
[19] D. Schroer, A. D. Greentree, L. Gaudreau, K. Eberl, L. C. L. Hollenberg, J. P. Kotthaus, and S. Ludwig, Phys. Rev. B **76**, 075306 (2007).
[20] M. Korkusinski, I. P. Gimenez, P. Hawrylak, L. Gaudreau, S. A. Studenikin, and A. S. Sachrajda, Phys. Rev. B **75**, 115301 (2007).
[21] M. C. Rogge and R. J. Haug, Phys. Rev. B **77**, 193306 (2008).
[22] S. Amaha, T. Hatano, S. Teraoka, A. Shibatomi, S. Tarucha, Y. Nakata, T. Miyazawa, T. Oshima, T. Usuki, and N. Yokoyama, Appl. Phys. Lett. **92**, 202109 (2008).
[23] L. Gaudreau, A. Kam, G. Granger, S. A. Studenikin, P. Zawadzki, and A. S. Sachrajda, Appl. Phys. Lett. **95**, 193101 (2009).
[24] S. Amaha, T. Hatano, T. Kubo, S. Teraoka, Y. Tokura, S. Tarucha, and D. G. Austing, Appl. Phys. Lett. **94**, 092103 (2009).
[25] E. A. Laird, J. M. Taylor, D. P. DiVincenzo, C. M. Marcus, M. P. Hanson, and A. C. Gossard, Phys. Rev. B **82**, 075403 (2010).
[26] T. Takakura, M. Pioro-Ladrière, T. Obata, Y.-S. Shin, R. Brunner, K. Yoshida, T. Taniyama, and S. Tarucha, Appl. Phys. Lett. **97**, 212104 (2010).
[27] L. Gaudreau, G. Granger, A. Kam, G. C. Aers, S. A. Studenikin, P. Zawadzki, M. Pioro-Ladrière, Z. R. Wasilewski, and A. S. Sachrajda, Nat. Phys. **8**, 54 (2012).
[28] G. Shinkai, T. Hayashi, T. Ota, and T. Fujisawa, Phys. Rev. Lett. **103**, 056802 (2009); K. D. Petersson, C. G. Smith, D. Anderson, P. Atkinson, G. A. C. Jones, and D. A. Ritchie, *ibid.* **103**, 016805 (2009); I. van Weperen, B. D. Armstrong, E. A. Laird, J. Medford, C. M. Marcus, M. P. Hanson, and A. C. Gossard, *ibid.* **107**, 030506 (2011).
[29] M. Gibertini, A. Singha, V. Pellegrini, M. Polini, G. Vignale, A. Pinczuk, L. N. Pfeiffer, and K. W. West, Phys. Rev. B **79**, 241406(R) (2009); A. Singha, M. Gibertini, B. Karmakar, S. Yuan, M. Polini, G. Vignale, M. I. Katsnelson, A. Pinczuk, L. N. Pfeiffer, K. W. West, and V. Pellegrini, Science **332**, 1176 (2011).
[30] C. Nayak, S. H. Simon, A. Stern, M. Freedman, and S. Das Sarma, Rev. Mod. Phys. **80**, 1083 (2008).
[31] L. P. Kouwenhoven, T. H. Oosterkamp, M. W. S. Danoesastro, M. Eto, D. G. Austing, T. Honda, and S. Tarucha, Science **278**, 1788 (1997).
[32] T. Hatano, S. Amaha, T. Kubo, Y. Tokura, Y. Nishi, Y. Hirayama, and S. Tarucha, Phys. Rev. B **77**, 241301(R) (2008).
[33] T. Fujisawa, D. G. Austing, Y. Tokura, Y. Hirayama, and S. Tarucha, J. Phys. Condens. Matter **15**, R1395 (2003).
[34] T. Hatano, M. Stopa, and S. Tarucha, Science **309**, 268 (2005).
[35] See Supplemental Material at http://link.aps.org/supplemental/10.1103/PhysRevB.85.081301 for additional data and calculations.
[36] J. R. Petta, A. C. Johnson, J. M. Taylor, E. A. Laird, A. Yacoby, M. D. Lukin, C. M. Marcus, M. P. Hanson, and A. C. Gossard, Science **309**, 2180 (2005); J. R. Petta, H. Lu, and A. C. Gossard, *ibid.* **327**, 669 (2010).